Journal of Nuclear Materials 392 (2009) 420–426

Contents lists available at ScienceDirect

Journal of Nuclear Materials

journal homepage: www.elsevier.com/locate/jnucmat

Low-temperature mechanical properties of superconducting radio frequency cavity materials

Thak Sang Byun *, Sang-Ho Kim, John Mammosser

Oak Ridge National Laboratory, P.O. Box 2008, Oak Ridge, TN 37831, United States

ARTICLE INFO

Article history:
Received 25 February 2009
Accepted 31 March 2009

ABSTRACT

Low-temperature mechanical behaviors have been investigated for the constituent materials of superconducting radio frequency cavities. Test materials consist of small grain Nb, single crystal Nb, large grain Nb (bicrystal), Ti45Nb–Nb weld joint (e-beam welded), and Ti–316L bimetal joint (explosion welded). The strength of all test metals displayed strong temperature dependence and the Ti–316L bimetal showed the highest strength and lowest ductility among the test materials. The fracture toughness of the small grain Nb metals decreased with decreasing test temperature and reached the lower shelf values (30–40 MPa $\sqrt{m}$) at or above 173 K. The Ti45Nb base and Ti45Nb–Nb weld metals showed much higher fracture toughness than the small grain Nb. An extrapolation and comparison with existing data showed that the fracture toughness of the small grain Nb metals at 4 K was expected to be similar to those at 173 and 77 K. The results from optical photography at a low magnification and fractography by a scanning electron microscope were consistent with corresponding mechanical properties.

Published by Elsevier B.V.

1. Introduction

The radio frequency cavities are used to accelerate charged particles to high speeds. Recently, the use of superconducting radio frequency (SRF) cavities has become widespread in particle accelerators [1–6], and the typical operating temperature of SRF cavities is between 2.1 and 4.2 K. The SRF cavities are usually serially connected elliptical shells to resonate high frequency electrical fields and are made of pure niobium with high residual resistivity ratio (RRR) (>200) [7–16], along with other adjoining metallic materials such as austenitic stainless steels, titanium, and titanium alloys [7,13–18].

The cryogenic component also includes various joining structures such as the Nb–Nb electron-beam weld joint, Ti45Nb–Nb weld joint, and Ti–316L bimetal joint (explosion welded). Since the niobium cavities and other structures are operated at or below liquid helium temperature and most of the cavity constituent materials are expected to be in or near the lower shelf fracture toughness region, there has been a concern on their structural integrity [1,7–9,11,12]. The structural safety of the cavities cannot be assured unless all of the constituent materials retain a proper level of strength, ductility, and fracture toughness during normal operation, including thermal cycles between room temperature and operating temperature, as well as on accidental situations.

Regardless of its relatively small size, a cavity is built of multiple materials and weld joints, and therefore the evaluation of its mechanical integrity requires complex considerations on mechanical properties for base metals and weld joints. It is well known that the body-centered cubic metals like Nb experience a ductile-to-brittle transition at a low temperature [7,8,19], and the main constituent material of SRF cavities, pure Nb, is known to have a ductile-to-brittle transition temperature (DBTT) above the liquid helium temperature [7,8]. In such a case, the lower shelf fracture toughness is considered as the key property for the integrity assessment of the cryogenic system. Meanwhile, the fracture toughness of high purity Ti is slightly higher than that of high purity Nb at cryogenic temperatures [7] and other cavity materials such as austenitic stainless steels have significantly higher fracture toughness. For some of the higher ductility materials, the fracture toughness based analysis may not always be useful for structural integrity assessment because the wall thickness of a SRF cavity is of the order of a few to several millimeters and the fracture toughness from such a thin ductile structure cannot satisfy the thickness requirements for valid fracture toughness values [20,21]. It is therefore expected that, for some constituent materials, the assessment procedure should rely more on the ductility data from uniaxial tensile testing. Another consideration is the influence of material chemistry and manufacturing processes. The ultra-high purity of Nb and Ti and the unique manufacturing processes to produce high RRR materials make it more difficult to utilize known material property databases. Furthermore, the joining processes such as the electron-beam welding and explosion welding produce narrow melt and heat-affected zones, from which taking specimens for testing individual materials is often not possible, and as a result, the basic mechanical properties of these joints are largely

* Corresponding author. Tel.: +1 865 576 7738.
E-mail address: byunts@ornl.gov (T.S. Byun).

0022-3115/$ - see front matter Published by Elsevier B.V.
doi:10.1016/j.jnucmat.2009.03.058

unknown. For the SRF cavity base materials, however, none of the primary mechanical properties has been thoroughly evaluated. A scoping experiment on the mechanical properties of the cavity materials has been suggested to determine the way of integrity analysis and to provide basic data for assessing the integrity.

This study aimed at the evaluation of mechanical properties for selected cavity materials at low temperatures ranging from room temperature to liquid nitrogen temperature. Tensile tests and fracture toughness tests were performed in static conditions for selected SRF cavity materials. Fractography in a scanning electron microscope (SEM) was performed for the broken fracture specimens to examine fracture mode and confirm mechanical behavior at each temperature. Also, the necked and/or fractured tensile specimens were photographed at low magnification to characterize the necking and final fracture features of test materials. For the obtained mechanical properties, analysis is made focusing on temperature dependence, and the results are used to predict the properties at liquid helium temperature, which will be produced in the next experimental campaign.

2. Experiment

Coupons taken from SRF cavities or model material disks were used for machining tensile and fracture specimens in as-received conditions. Information on the test materials is summarized in Table 1. For tensile tests, SS-3 type specimens with the gage section dimensions of $1.5 \times 7.6 \times 0.76$ mm were machined from base metals and weldments [22,23]. The base metal specimens include commercially rolled and recrystallized Nb specimens (small grain Nb specimens: Nb-30 and Nb-T30), single crystal Nb specimens, and large grain (bicrystal) Nb specimens. The weldment specimens were taken from the electron-beam welded Ti45Nb–Nb joint and explosion welded Ti–316L joint, which include the melt region (fusion line) at the middle of the gage section and the base metals (Nb, Ti45Nb, Ti, and 316L) next to narrow heat-affected zones (HAZs). As will be discussed later, the deformation characteristics in these weldment specimens will be largely represented by the weaker portion of the joints, i.e., Nb and 316L regions.

Two types of subsized specimens were machine for the fracture toughness tests: the disk compact tension (DCT) specimens of 12.5 mm diameter and 4.14 mm thickness for small grain base metals (Nb-30 and Nb-T30), and single edge (three-point) bend (SEB) specimens with dimensions of $5 \times 5 \times 25$ mm for the Ti45Nb base metal and Ti45Nb–Nb weld metal. Note that the Ti45Nb alloy is a transitional metal from Nb to Ti and the Ti45Nb–Nb weld metal is a narrow mixed metal zone formed by melting during e-beam welding process. It was possible to produce precrack in the Ti45Nb–Nb melt region in spite of its small size. However, introduction of a precrack was not possible for the Ti–316L weldments because the melt zone was much narrower and its wall thickness was too thin, and therefore the fracture toughness was not measured for the Ti–316L weld joints. In the weldment specimens the specimen orientation in the plates was taken so that crack propagation occurs in the S direction (or surface normal direction on the plate). In other specimens the cracks were made along the surface normal direction. Detailed specimen configurations are described in the ASTM standard testing methods [20,21]. For both tensile and fracture tests, the temperature control between room temperature and liquid nitrogen temperature was made by a solenoid valve controlled injection of liquid nitrogen into the testing chamber. For 77 K tests, the specimens were immersed in a liquid nitrogen bath.

Tensile tests were performed using a screw-driven Instron machine at temperatures ranging from room temperature (RT) to 77 K at a nominal strain rate of $\sim 2 \times 10^{-3}$ s^{-1} (cross head speed = 0.017 mm/s). The load-elongation data were analyzed using a program based on ASTM standard E8 [22]. After testing the fractured pairs of tensile specimens were photographed to compare the shapes of necks and fractured ends.

For fracture toughness tests, the DCT and SEB specimens whose initial notch length-to-width ratios were 0.36 and 0.4, respectively, were fatigue pre-cracked at 20 Hz to produce sharp cracks until the crack length-to-width ratios (a/w) reached 0.44–0.57 [20,21]. Fracture tests were performed in a MTS servo-hydraulic machine or a screw-driven machine at a cross head speed of 0.005 mm/s. Fracture toughness testing and analysis were performed based on the procedures and recommendations dictated by the ASTM standard E1820, standard test method for measurement of fracture toughness [21]. The load versus load-line displacement curves were recorded and analyzed to determine crack growth and fracture toughness using the unloading compliance method or normalization method, depending on the ductility of specimen. Interim fracture toughness values, K_Q, were determined when the load–displacement curve indicated unstable crack growth, while J_Q values were determined when the curve indicated crack blunting or stable crack growth. The interim fracture toughness values were verified using selected ASTM criteria, however, as mentioned in the next section, many fracture toughness data are invalid mainly because of the small specimen sizes tested.

Initial and final crack lengths were measured from the optical photographs of fracture surfaces and used in the calculation of

Table 1
Test materials, their chemistry, and related information.

#	Material/ joint	Chemistry (in wt%, otherwise specified)	Remarks
1	Nb-T30 (small grain)	Nb (total impurity < 0.06, Ta < 0.044)	Commercially rolled and recrystallized Tokyo Denki pure niobium, high residual resistivity ratio (RRR), average grain size = 55 μm [1], crack growth parallel to the surface
2	Nb-30 (small grain)	Nb (total impurity < 0.07, Ta < 0.036)	Commercially rolled and recrystallized Wah Chang pure niobium, high RRR, average grain size = 40 μm [1], crack growth parallel to the surface
3	Ti45Nb–Nb weld joint	Nb(bal)–55.3Ti–0.108Zr–0.05Ta–0.025Mo–0.01Fe–0.007 W/ Nb (total impurity < 0.07)	Ti45Nb/nuclear grade Nb, electron-beam welded, tensile direction normal to the welding line, crack growth to the surface normal direction in both weld (melt) and Ti45Nb specimens
4	Ti–316L weld joint	Ti(bal)–0.1Fe–0.01C–0.17O–0.01 Ni/Fe(bal)-16.839Cr–10.535Ni–2.531Mo–1.843Mn-0.189Cu–0.024C–0.028P–0.011N	Annealed Ti grade 2/annealed 316L, specimen taken from joined piping, explosion welded, tensile direction normal to the welding line
5	Nb-single crystal (T)	Nb (Ta ~ 0.08)	Specimens taken from a disk sliced from large grain ingot (CBMM Co, 280–300 mm diameter [1]), tensile direction = transverse (T) or circumferential direction, grain size up to 100 mm
6	Nb-single crystal (R)	Nb (Ta ~ 0.08)	Specimens from the same disk, tensile direction = radial (T) direction
7	Nb-bicrystal (large grain)	Nb (Ta ~ 0.08)	Specimens from the same disk, tensile direction = normal to a grain boundary

fracture toughness. Also, SEM fractography was performed on the fracture surfaces of the specimens tested at room temperature, 173 and 77 K. The SEM images were used to confirm the consistency between the fracture mechanisms and the fracture toughness values.

3. Results and discussion

3.1. Temperature dependence of strength and ductility

As seen in Figs. 1 and 2, the yield and ultimate tensile strengths decrease monotonically with temperature, while the uniform and total elongations increase with temperature. The strengths of the test materials, except for the explosion welded Ti–316L bimetal, fall within a narrow band, while the elongations showed larger variations among materials. In particular, the elongations for weld joints were much lower than those for base metals. This may be because the deformation in weld joints is significantly uneven around the weld. In the Ti45Nb–Nb weld material, peak deformation is observed on the Nb side of the HAZ or near the HAZ. Since this weld zone is a melt mixture of the Ti45Nb alloy and pure Nb formed by electron-beam heating, the strength measured from the Ti45Nb–Nb weld joint is actually a composite strength for the joint. Thus, it should represent more of the softest part of the joint, while the relatively low ductility represents a highly concentrated deformation in the lowest strength portion of the joint or in the nuclear grade Nb or HAZ.

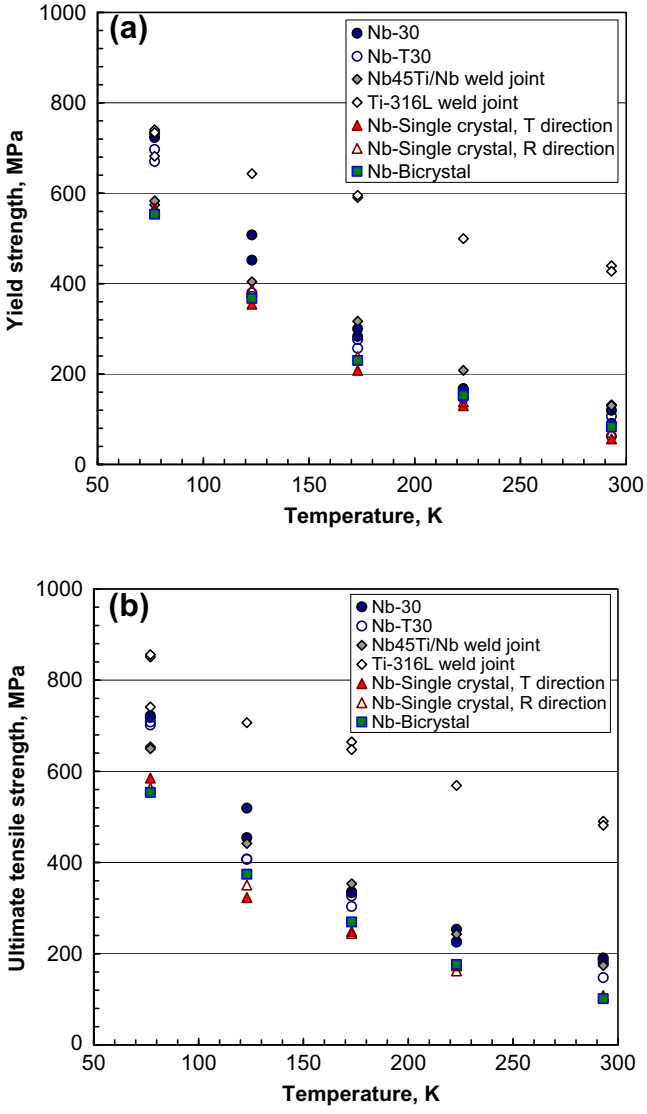

Fig. 1. Temperature dependence of strengths in niobium materials and weld joints: (a) yield strength and (b) ultimate tensile strength.

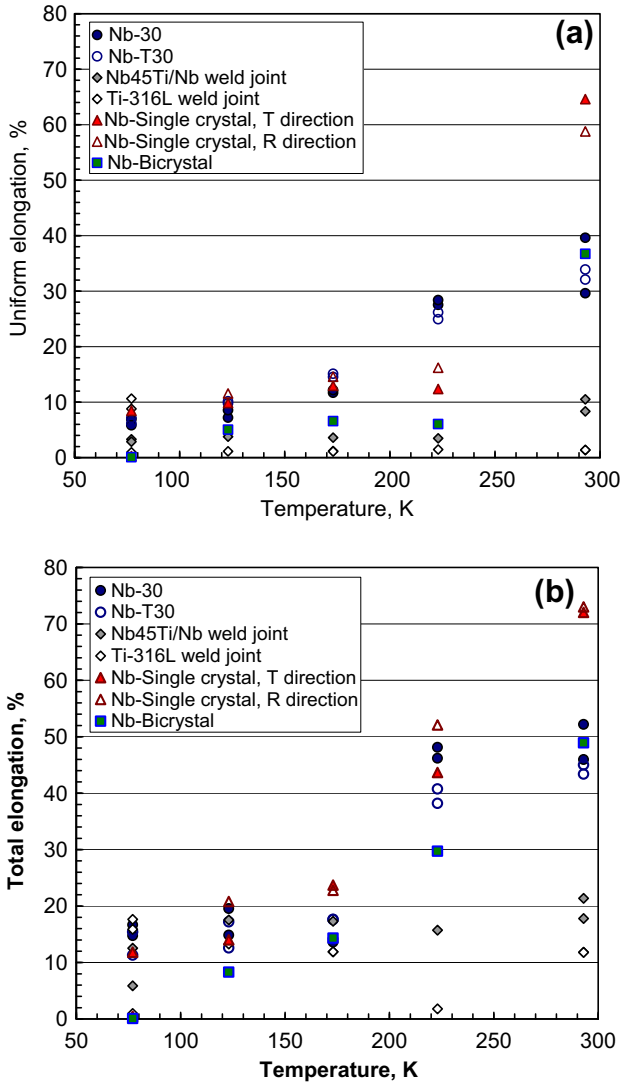

Fig. 2. Temperature dependence of ductility in niobium materials and weld joints: (a) uniform elongation and (b) total elongation.

In the two components of the Ti–316L bimetal joint, the explosion welding process might have produced a plasticity zone with a higher dislocation density upon impact, resulting in the highest strength among the test materials. The specimens broke either at the neck in weaker Ti region with significant plasticity or at the joint (or interface) after small or little plastic deformation in the Ti section of the specimen. This indicates that the measured ultimate tensile strength (UTS) is close to the joining strength achievable from the explosion weld method. Although the ductility in this joint is not high, the result shows that the joint strength is high enough to prevent a failure at the interface prior to experiencing significant plasticity or failure at other parts of the cavity. Also, it is worth recognizing that, at least to the liquid nitrogen temperature, the Ti–316L joint does not experience complete embrittlement but shows a continuous increase of joint strength with decreasing temperature, which indicates that plasticity still has a significant role in the failure process.

While relatively small differences were found among the strengths of the materials without weld joint (Nb-30, Nb-T30, single crystal Nb, and bicrystal Nb) the ductility data showed larger variations over the test temperature range. The bicrystal Nb, in particular, presents the lowest elongations among these metals but its strength falls within the same band. This indicates that the grain boundary at the middle is detrimental to the ductility of Nb, probably due to a grain boundary weakening mechanism such as segregation of alloy elements or impurities. In the typical polycrystalline Nb materials, such segregation of elements, if any, can be diluted at abundant grain boundaries, and therefore the ductility can be recovered. The grain size of this material is of the order of a few centimeters, and the electro-magnetic properties with such large or single grain material could be beneficial for the performance of the device. However, from the point of view of mechanical properties, using such a large grain material will result in less structural safety.

3.2. Necking and failure modes

The tensile failure made can be well characterized by the shape of necked and fractured region. Figs. 3–6 display the pairs of fractured tensile specimens, of which the features are consistent with the tensile data described above. In Fig. 3, the small grain Nb-30 shows typical necked and fractured shapes: the angle of localized neck and final shear to the loading direction seems to decrease with decreasing test temperature and total elongation increased with temperature. In Fig. 4, the single crystal and bicrystal Nb specimens show similar necking and shear failure behaviors at all test temperatures. The necks are significantly elongated before final failure at room temperature, and the length of the necked region decreased or nearly disappeared at 77 and 173 K. The necking angle also decreased with decreasing test temperature. The reduced necking and failure in nearly brittle manner along grain boundary at these low temperatures confirms that having small amount of grain boundary in Nb is detrimental.

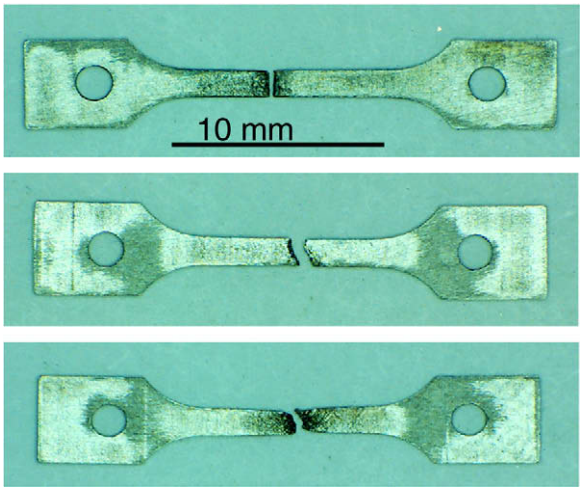

Fig. 3. Necking and final fracture in Nb-30 base metal tested at 295, 173, and 77 K (from the top).

In the Ti45Nb–Nb weldment specimens (Fig. 5), the heavy deformation in the necked region revealed metallurgically different zones: the weld zone and base metal regions. In particular, the boundary between the weld metal and the harder base metal (Ti45Nb alloy) is discernable from the Ti45Nb base metal region due to the severe deformation in the weld region. Necking or plastic instability occurred over the weld zone and Nb base metal region; the narrowest neck and final fracture occurred around the weld metal–base metal boundary or heat-affected zone on the Nb side, which is very narrow.

It is seen in Fig. 6 that final failure occurred along the grain boundary at 77 and 173 K. In the Ti–316L bimetal specimens, the final failure occurred either at the joint region or at the neck formed in the Ti region (darker side). The location of final failure was not consistent; the normal necking failure occurred in the Ti region at RT, 77, and 173 K, while nearly brittle failure occurred at the joint at 77 and 223 K. This brittle fracture behavior is reflected in the tensile ductility data Fig. 2.

3.3. Temperature dependence of fracture toughness

The fracture toughness test results for the base metal and weld metal specimens are presented in Fig. 7, and compared with the results from earlier studies for relevant materials [7,13,15,17]. The small grain Nb-30 and Nb-T30 base metals present nearly identical fracture toughnesses (K_Q) at the three test temperatures and show a steep transition between 173 K and room temperature. The other two materials, Ti45Nb–Nb weld and Ti45Nb base metals, showed higher fracture toughness values and more gradual transitions. The fracture toughness of the two Nb metals had already reached

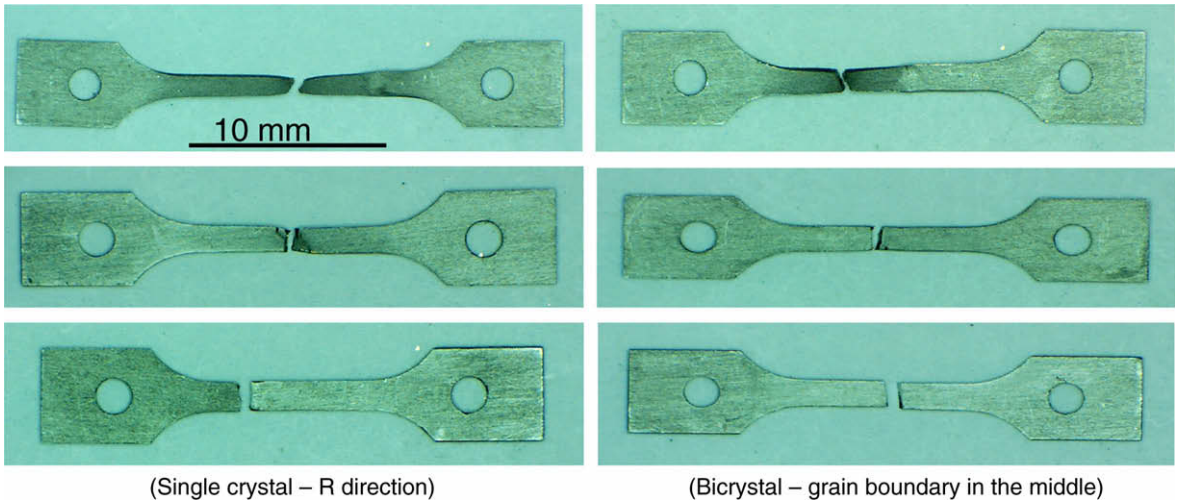

Fig. 4. Necking and final fracture in single and bicrystal specimens tested at 295, 173, and 77 K (from the top).

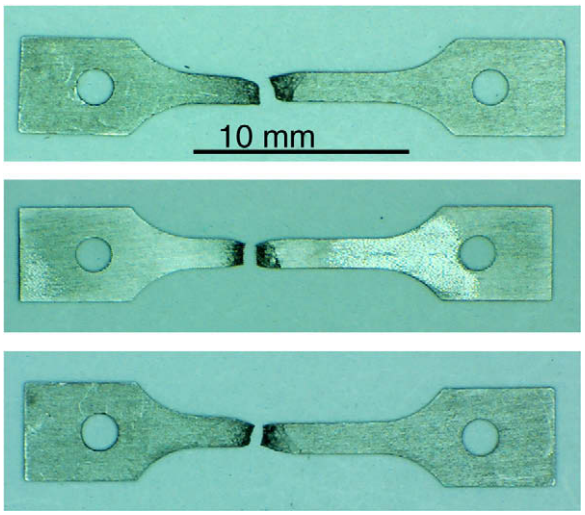

Fig. 5. Necking and final fracture in Ti45Nb–Nb weld joint tested at 295, 173, and 77 K (from the top). Necked and fracture occurred around the weld metal-Nb boundary.

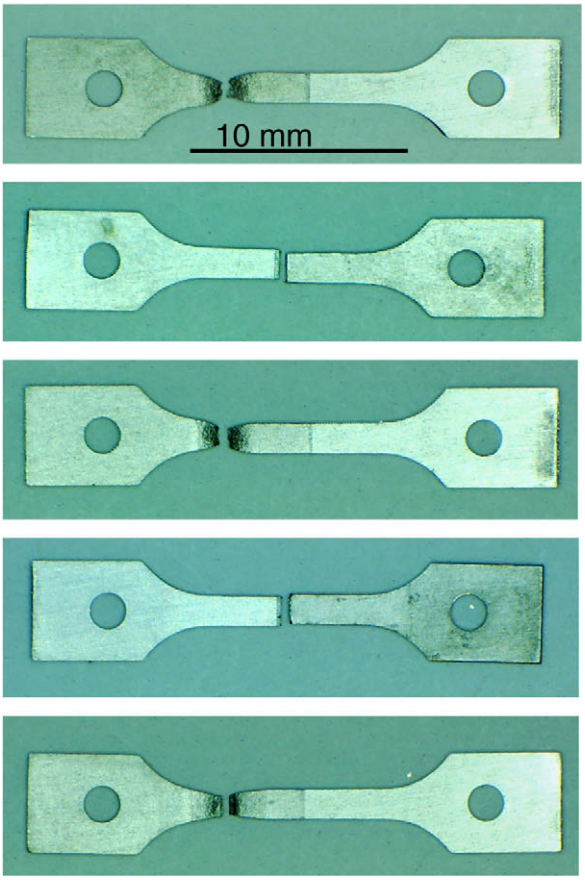

Fig. 6. Necking and final fracture in Ti–316L bimetal tested at 295, 123, 173, 77, and 77 K (from the top). Necked (darker) side is Ti.

their lower shelf level of 20–40 MPa $\sqrt{m}$ at 173 K and, as included in Fig. 7, the fracture toughness data for liquid helium temperature by Walsh et al. [7] lie on the extrapolated curve of the data from this study. It is therefore expected that similar fracture toughness values would be measured for the Nb metals currently being examined at the liquid helium temperature. In the 173 K tests, stable crack extension over 2 mm occurred in both Nb metals. Although

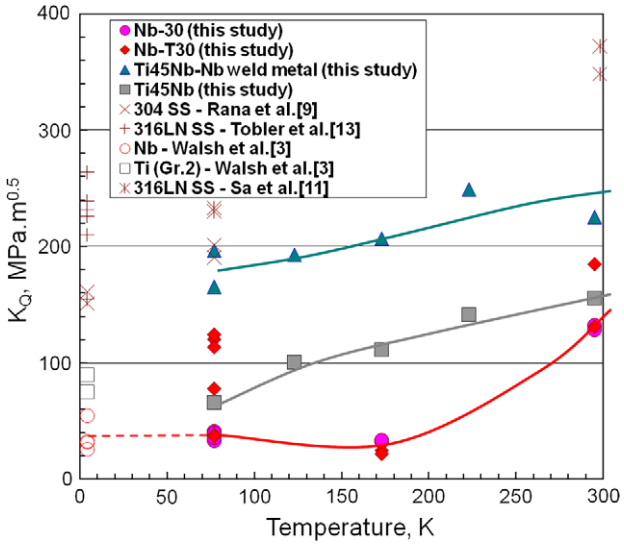

Fig. 7. Temperature dependence of fracture toughness in cavity weld materials. (The room temperature data for Nb-30, Nb-T30, and Ti45Nb–Nb weld and the 223 K data for Ti45Nb–Nb weld cannot satisfy the size requirement.)

such a stable crack extension can imply significant plasticity at crack tip, rather low fracture toughness values were measured: about 33 MPa $\sqrt{m}$ for Nb-30 and 22 and 25 MPa $\sqrt{m}$ for Nb–T30. In room temperature tests, however, much higher fracture toughness values (>120 MPa $\sqrt{m}$) were measured for both metals.

Although similar temperature dependences were observed for the two high RRR small grain Nb metals in the low-end fracture toughness data, detailed fracture behaviors at 77 K are different if we include all invalid test cases. Six tests were performed for each material at 77 K, and shown in Fig. 7. All six specimens from the Nb-30 plate fractured without noticeable ductility and showed low fracture toughness (K_Q) in a narrow range of 33–42 MPa $\sqrt{m}$ (six data points are clustered in Fig. 7). A few of the Nb-T30 specimens, however, experienced significant crack blunting, and consequently the data are dispersed in a wide range of 37–125 MPa $\sqrt{m}$. Among these Nb-T30 specimens, two specimens fractured in elasticity range at 77 K, while the other four showed significant crack-tip plasticity and blunting with little crack extension. Inhomogeneous microstructure and relatively small specimen size are believed to be responsible for such a wide discrepancy in fracture behavior. Among the fracture toughness measurements for Nb-30, the two lowest values, 37 and 38 MPa $\sqrt{m}$, were valid, but four higher values, about 80 or 120 MPa $\sqrt{m}$ turned out to be invalid due to excessive plasticity or lack of crack growth [20,21].

It should be noted that the room temperature data for Nb-30, Nb-T30, and Ti45Nb–Nb weld and the 223 K data for Ti45Nb–Nb weld are not valid because the specimen size (thickness or initial crack size) cannot satisfy the size requirement of relevant ASTM standards [20,21]. In these subsized specimens, crack blunting and lateral (thickness) contraction continued on testing without crack extension due to excessive ductility. For such cases, no complete *J*-resistance curve could be constructed and the fracture toughness from the specimen that satisfies the ASTM size requirements can be lower than the values displayed in Fig. 7.

A comparison among materials shows that the fracture toughnesses of the Ti45Nb–Nb weld metal and stainless steels are significantly higher than the base metals: Nb-30, Nb-T30, and Ti45Nb alloy. Since the Nb base metals show the lowest fracture toughness in the test temperature range, the mechanical integrity of a cavity vessel is believed to be largely determined by the Nb base metals. It should be also noted that the data for the Ti45Nb alloy at 77 K (66 MPa $\sqrt{m}$) is significantly reduced from the data at higher

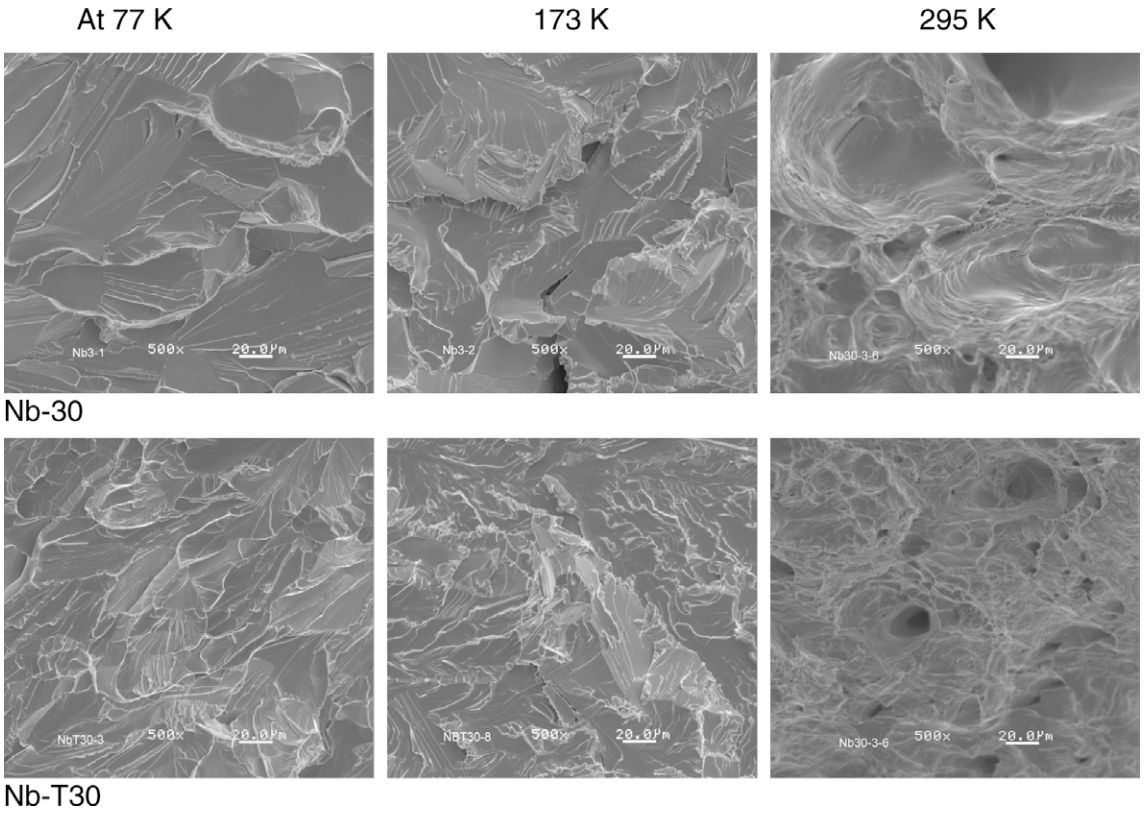

Fig. 8. SEM fractographs for high RRR Nb metals. (Scale markers indicate 20 μm; note that the specimen I.D. within the last photograph is a mistake.)

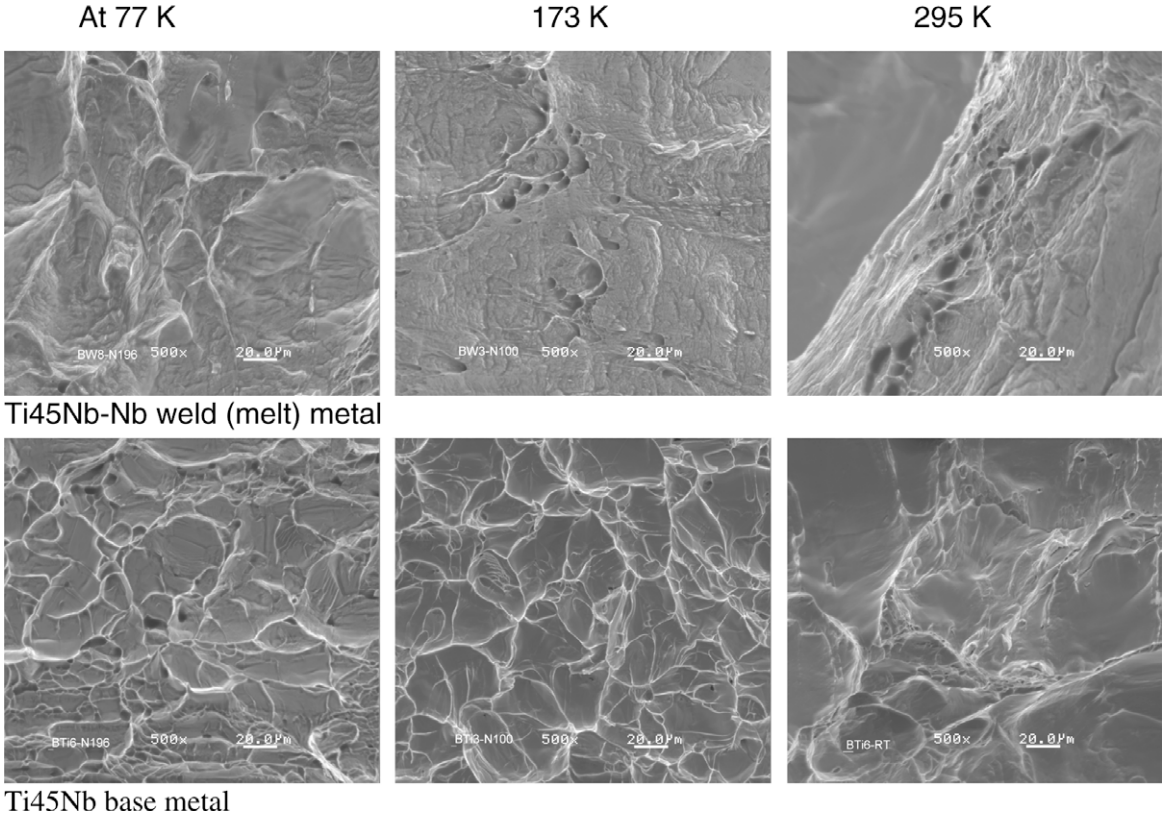

Fig. 9. SEM fractographs for Ti45Nb–Nb weld and Ti45Nb base metals. (Scale markers indicate 20 μm.)

temperatures and the fracture toughness of this alloy is expected to reach a lower value (or lower shelf level) at a lower temperature. Therefore, the Ti45Nb alloy, along with the pure Nb base metals, should be considered as a critical component material that would determine the mechanical integrity of SRF cavity.

3.4. Fracture surface

The SEM images in Figs. 8 and 9 illustrate the temperature and materials dependences of fracture surface in the base and weld materials. Note that the fracture surface images were taken from a crack growth area near the boundary between the fatigue-precrack and crack growth areas. These facture surface features correctly reflect the corresponding fracture toughness values in Fig. 7. For Nb-30 and Nb-T30, the fracture surfaces obtained from 77 to 173 K contain cleavage facets and river-patterned shear ribs, which are typical features obtained in the lower shelf region Fig. 7. The fracture surfaces from room temperature tests for both materials show typical ductile fracture surfaces with large and small dimples. Some large holes, which are usually considered as the crack or large dimple initiation sites, often coincide with the sites of relatively brittle precipitates. Also, SEM fractographs usually reflect some of the microstructural aspects of test materials. A comparison of the fracture surfaces from the two high RRR Nb metals revealed that the fractography features from Nb-T30 were finer than those from Nb-30, indicating the original subgrain structures of the Nb-T30 were finer.

The fractographs in the first row in Fig. 9 are for the Ti45Nb–Nb weld metal and display totally ductile fracture features throughout the test temperature range. These show dimpled surfaces; however, the dimples are shallow and are elongated by shear. Due to its very high toughness and ductility, the specimens were not separated until they experienced significant crack tip blunting. At room temperature, the blunting was so severe that the SEM imaging for large crack growth area could not provide typical fracture surfaces, as indicated in Fig. 9. As indicated in the fracture toughness level in Fig. 7, the fracture surface characteristics for the Ti45Nb alloy are between the Nb base metals and the Ti45Nb–Nb weld metal Fig. 9. Although these all show dimpled surfaces, the dimples are shallow, indicating that a relatively low energy fracture process has occurred in the material.

4. Conclusions

Mechanical tests have been performed to investigate the key mechanical properties of selected SRF cavity materials: high RRR small grain Nb metals, e-beam welded Ti45Nb–Nb joint, Ti45Nb base metal, single crystal Nb, large grain Nb (bicrystal), and explosion welded Ti–316L bimetal joint. The main findings and conclusions are as follows:

[1] The yield and ultimate tensile strengths of small grain Nb metals, Ti45Nb–Nb weld joint, and single and bi-crystals displayed strong temperature dependence while they fell within a narrow band. The explosion-welded Ti–316L specimens showed the highest strength among the tested metals, while showing the lowest ductility. Optical photography indicated that the necking and final fracture occurred either at the Ti side or at the joint in the bimetal specimens.

[2] The fracture toughness of small grain Nb metals decreased with decreasing test temperature and reached lower shelf values (30–40 MPa $\sqrt{m}$) below room temperature. An extrapolation and comparison show that the present fracture toughness data for Nb are consistent with those from earlier studies and the fracture toughness at 4 K is expected to be similar to those at 173 and 77 K.

[3] The Ti45Nb–Nb weld metal showed much higher fracture toughness than the base metal (Nb) and was still ductile at 77 K. The fracture toughness of Ti45Nb metal was also higher than that of Nb, but lower than the weld metal.

[4] Scanning electron microscopy (SEM) results were consistent with the fracture toughness results. Both the fracture toughness data and the fractography results confirmed that only the Nb base metals reached the brittle fracture condition, or lower shelf fracture toughness level well above the temperature of liquid helium.

[5] Mechanical testing in liquid helium (4 K) for the constituent materials of SRF cavities is needed for assessment of structural safety. Obtaining the fracture toughness data of the base metals, Ti45Nb and small grain Nb, is particularly important since their fracture toughnesses are found or expected to be in the lower shelf region at 4 K.

Acknowledgements

The study was sponsored by US Department of Energy, Offices of Basic Energy Science, under Contract DE-AC05-00OR22725 with UT-Battelle, LLC. The authors thank E. Manischmudt and A.M. Williams for their efforts for DCT fracture testing and SEM fractography. The authors also express special thanks to Drs Isidoro E. Campisi and David A. McClintock for their thorough reviews and thoughtful comments.

References

[1] S.H. Kim, I.E. Campisi, IEEE. Trans. Appl. Supercond. 17 (2007) 1299.
[2] D.A. Edwards, TESLA Test Facility Linac. Design Report, DESY Print TESLA Rep. 95-01.
[3] DESY XFEL Project Group, The European X-Ray Free Electron Laser Technical Design Report, DESY 2006-097.
[4] S. Nagaitsev, Fermilab's Project X, Presented in the XXIV Linear Accelerator Conference, Victoria, Canada, 2008..
[5] A. Yamamoto, in: Proceedings of European Particle Accelerator Conference, Genoa, Italy, 2008, p. 12.
[6] D. Baars, T.R. Bieler, K.T. Hartwig, H. Jiang, C. Compton, T.L. Grimm, J. Metals (June) (2007) 50.
[7] R.P. Walsh, R.R. Mitchell, V.T. Toplosky, R.C. Gentzlinger, in: Proceedings of 19th Workshop on RF Superconductivity, Santa Fe, USA, 1–5 November 1999.
[8] R.P. Walsh, K. Han, V.T. Toplosky, R.R. Mitchell, in: Proceedings of the International Cryogenic Materials Conference (ICMC), vol. 48, 2002, p. 186.
[9] K. Ishio, K. Kikuchi, J. Kusano, M.Mizumoto, K. Mukugi, A. Naito, N. Ouchi, Y. Tsuchiya, K. Saito, in: Proceedings of the ninth Workshop on RF Superconductivity, Santa Fe, New Mexico, USA, 1–5 November 1999.
[10] A. Zamiri, F. Pourboghrat, H. Jiang, T.R. Bieler, F. Barlat, J. Brem, C. Compton, T.L. Grimm, Mater. Sci. Eng. A 435&436 (2006) 658.
[11] M.G. Rao, P. Kneisel, in: Proceedings of the Sixth Workshop on RF Superconductivity, Newport News, Virginia, USA, 4–8 October 1993.
[12] E. Bemporad, F. Carassiti, M. Sebastiani, G. Lanza, V. Palmieri, H. Padamsee, Supercond. Sci. Tech. 21 (2008), doi:10.1088/0953-2048/21/12/125026.
[13] M.D. Rana, W.D. Doty, S. Yukawa, R. Zawierucha, Tran. ASME 123 (2001) 332.
[14] S.F. Kane, A.L. Farland, T.A. Siewert, C.N. McCowan, Welding Res. Supplement (August) (1999) 292.
[15] J.W. Sa, H.K. Kim, C.H. Choi, H.T. Kim, K.H. Hong, H.K. Park, J.S. Bak, K.W. Lee, E.T. Ha, in: 21st IEEE/NPS Symposium on Fusion Engineering 2005, Knoxville, Tennessee, USA, 26–29 September 2005.
[16] M.J. Morgan, G.K. Chapman, M.H. Tosten, S.L. West, Tritium Effects on Fracture Toughness of Stainless steel Weldments, WSRC-MS-2004-00579, Westinghouse Savannah River Site, Aiken, South Carolina, USA, 12 May 2005.
[17] R.L. Tobler, A. Nishimura, J. Yamamoto, Cryogenics 37 (1997) 533.
[18] K. Mukugi, N. Ouchi, A. Takemura, Y. Morimoto, in: Proceedings of the 10th Workshop on RF-Superconductivity, Tsukuba, September 2001.
[19] R.W. Hertzberg, Deformation and Fracture Mechanics of Engineering Materials, 3rd Ed., John Wiley and Sons, Inc., New York, 1989 (Chapter 9).
[20] ASTM Standard E 399: Standard Test Method for Plane-Strain Fracture Toughness of Metallic Materials.
[21] ASTM Standard E 1820: Standard Test Method for Measurement of Fracture Toughness.
[22] ASTM Standard E 8M: Test Method for Tension Testing of Metallic Materials.
[23] T.S. Byun, N. Hashimoto, K. Farrell, Acta Mater. 52 (2004) 3889.